Bulletin of Mathematical Biology (2022) 84:145
https://doi.org/10.1007/s11538-022-01100-9

Society for Mathematical Biology

ORIGINAL ARTICLE

Inhibitor-Induced Wavetrains and Spiral Waves in an Extended FitzHugh–Nagumo Model of Nerve Cell Dynamics

M. Osman Gani[1,2] · M. Humayun Kabir[1,2] · Toshiyuki Ogawa[3,4]

Received: 15 May 2022 / Accepted: 12 October 2022 / Published online: 9 November 2022

Abstract

It is well known that the FitzHugh–Nagumo model is one of the simplified forms of the four-variable Hodgkin–Huxley model that can reflect most of the significant phenomena of nerve cell action potential. However, this model cannot capture the irregular action potentials of sufficiently large periods in a one-parameter family of solutions. Motivated by this, we propose a modified FitzHugh–Nagumo reaction-diffusion system by changing its recovery kinetics. First, we investigate the parameter regime to know the existence of the wavetrains. Second, we conceive the occurrence of Eckhaus bifurcations of solutions that divide the solution region into two parts. The essential spectra at different grid points explore the occurrence of bifurcations of the waves. We find that the wavetrains of sufficiently large periods cross the stability boundary. This characteristic phenomenon is absent in the standard FitzHugh–Nagumo model. Finally, we observe a reasonable agreement between the direct PDE simulations and the solutions in the traveling wave ODEs. Furthermore, the model exhibits spiral wave for monotone and non-monotone cases that agrees with the waves observed in cellular activity.

Modeling, Analysis, and Simulation of Biological Systems (in memory of Masayasu Mimura).

✉ M. Osman Gani
osmangani2@juniv.edu

M. Humayun Kabir
hkabirju@gmail.com

Toshiyuki Ogawa
tshogw@gmail.com

1 Mathematical and Computational Biology (MCB) Research Group, Department of Mathematics, Jahangirnagar University, Dhaka 1342, Bangladesh

2 Center for Mathematical Modeling and Applications (CMMA), Meiji University, Tokyo 164-8525, Japan

3 Graduate School of Advanced Mathematical Sciences, Meiji University, 4-21-1, Nakano-ku, Tokyo 164-8525, Japan

4 Meiji Institute for Advanced Study of Mathematical Sciences, Meiji University, 4-21-1 Nakano, Nakano-ku, Tokyo 164-8525, Japan

Keywords Wavetrains · Extended FitzHugh–Nagumo model · Essential spectrum · Eckhaus bifurcation · Oscillating wavetrains

Mathematics Subject Classification 35K57 · 35Q92 · 92B25 · 65P20 · 65P30

1 Introduction

Wavetrain or periodic traveling wave (PTW) is a significant characteristic for a solution of nonlinear partial differential equations (PDEs) in excitable media (Meron 1992). Nerve cell dynamics, population dynamics, and cardiac cell dynamics are some examples of excitable media. The corresponding periodic solution of the PDEs is the spiral wave and scroll wave in two-space and three-space dimensions, respectively. Wavetrain was first identified in a reaction-diffusion system in 1973 by Kopell and Howard (1973). Later, it becomes an important topic of research in excitable systems. The PTWs were also identified in several real systems such as chemical reactions (Epstein and Showalter 1996; Vanag and Epstein 2008; Bordyugov et al. 2010), biological systems (DeVille and Eijnden 2007; Sherratt and Lord 2007), physical systems (Steinberg et al. 1989; Hecke 2003; Saarloos 2003), and ecological systems (Ranta and Kaitala 1997; Bierman et al. 2006; Sherratt and Smith 2008). A real system always has at least two characteristic phenomena: regular and irregular. So, it is important to study both regular and irregular behavior of wavetrains in a real system. It is truly believed that the dynamics of the nerve cells produce action potentials periodically. Moreover, spiral phenomenon is observed in numerous physiological systems, e.g., cardiac ventricular fibrillation (Davidenko et al. 1992; Gani and Ogawa 2014), retinal spreading depression (Gorelova and Bureš 1983), glial calcium in cortical tissue culture (Verkhratsky et al. 1998), and nerve cell dynamics (Ermentrout and Kleinfeld 2001a). To understand the dynamical behaviors of those systems, it is merely important to investigate the occurrence of the spiral wave, which can reflect the real scenario of wave phenomena in different systems. Mathematical model-aided understanding of the occurrence of spiral waves in biological systems is becoming an active topic to the researchers (Huang 2004).

The FitzHugh–Nagumo (FHN) model is a reaction-diffusion system with two unknowns in excitable media (FitzHugh 1961; Nagumo et al. 1962), which is one of the simplified forms of the four-variable Hodgkin–Huxley model. In 1952, Hodgkin and Huxley first proposed a mathematical model for the study of action potential propagation of the nerve cell dynamics in a squid giant axon. Among others, Hodgkin–Huxley (HH), FHN, and Hindmarsh–Rose (HR) models are most successful to conceive neural firing phenomena from a computational neuroscience viewpoint (Izhikevich 2007). However, a two-variable FHN model can capture the same characteristics behavior of action potential in the nerve cell. FHN is treated as the minimal model exhibiting significant features of nerve cells on account of its mathematical simplicity. In particular, the FHN model perceives excitable variables, that is, the membrane potential that demonstrates a fast dynamical behavior, the slow dynamical behavior, and it causes neurons' obstinate behavior. The simplified version from the four state variables HH model to the two-state variables FHN model concentrate on an empirical study on

the characteristics of excitation and propagation, while some distinct electrochemical features of the sodium and potassium ion flow are over-sighted (Oreanu et al. 2000). The drawback of this model is that it is not capable of producing unstable PTWs having sufficiently large periods (Gani and Ogawa 2015). Apart from the single neuron activity, wavetrains in neuroscience have undeniable importance at the tissue scale observed with neuroimaging techniques, e.g., electroencephalography (EEG). Such wavetrains occur due to an effect of local neuronal activity and synaptic interplay (Ermentrout and Kleinfeld 2001b). Previous studies on the understanding of existence and stability of PTWs dealt with the ionic models (Bauer et al. 2007; Echebarria et al. 2011; Sakaguchi and Maruyama 2008) and partial differential equation models (modified Barkley model (Bär and Brusch 2004), oregonator model (Bordiougov and Engel 2006; Bordyugov and Engel 2006)). However, they did not find any unstable PTWs of sufficiently large periods in their modifications of the FHN model. In this paper, we propose a modification in the classical FHN model and discuss the occurrence and instability of wavetrains for large periods in a parameter regime via the continuation package WAVETRAIN: a software package for investigating periodic traveling wave solutions of partial differential equations (Sherratt 2012).

The remaining part of the paper is arranged in the following manner. We present our proposed model and method of computation regarding the existence and stability of the wavetrains in Sect. 2. Section 3 represents the numerical simulation results and discussions in the model. We show the results in the proposed model in both monotone and non-monotone cases. Furthermore, the occurrence of spiral waves in the modified model for monotone and non-monotone cases justifies the waves of neuronal activity. Finally, we discuss the significant findings and conclusion of the paper in Sect. 4.

2 Model and Computation Technique

2.1 Model

The standard FitzHugh–Nagumo (FHN) model FitzHugh (1961); Nagumo et al. (1962) has equations of the form:

$$\begin{aligned} \frac{\partial u}{\partial t} &= d_u \left(\frac{\partial^2 u}{\partial x^2} + \frac{\partial^2 u}{\partial y^2} \right) + u(1-u)(u-a) - v, \\ \frac{\partial v}{\partial t} &= d_v \left(\frac{\partial^2 v}{\partial x^2} + \frac{\partial^2 v}{\partial y^2} \right) + \varepsilon(u - \gamma v). \end{aligned} \tag{1}$$

Here $u(t, \boldsymbol{x})$ represents membrane potential (activator variable) and $v(t, \boldsymbol{x})$ represents gating variable (inhibitor variable), where d_u and d_v represent diffusion rate of activator and inhibitor, respectively. The parameters a, ε, γ, d_u and d_v are assumed to be non-negative.

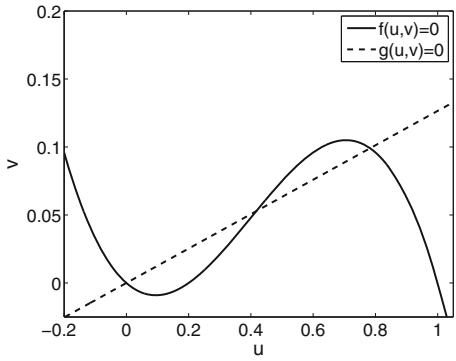

Fig. 1 Nullclines of the model (1). The parameters are the same as in Table 1

We have modified the FHN equations as the following:

$$\begin{aligned} \frac{\partial u}{\partial t} &= d_u \left(\frac{\partial^2 u}{\partial x^2} + \frac{\partial^2 u}{\partial y^2} \right) + u(1-u)(u-a) - v, \\ \frac{\partial v}{\partial t} &= d_v \left(\frac{\partial^2 v}{\partial x^2} + \frac{\partial^2 v}{\partial y^2} \right) + \varepsilon G_b(u - \gamma v), \end{aligned} \tag{2}$$

where the kinetics of the unknowns u and v are $f(u, v) = u(1-u)(u-a) - v$ and $g(u, v) = \varepsilon G_b(u - \gamma v)$, respectively. The variable u is regarded as the fast or activator variable, and v is regarded as the slow or inhibitor variable. Figure 1 shows the nullclines of the classical FHN model (1). The u-nullcline of the modified FHN model (2) is the same as the standard FHN model (FitzHugh 1961; Nagumo et al. 1962). We have modified the v-nullcline by the help of a scaled function $G_b(x)$.

The function $G_b(x)$ can be obtained from a given function $G(x)$, that is,

$$G_b(x) = \frac{G(bx)}{b},$$

where b is a positive parameter. If a smooth function $G(x)$ has the following property:

(i) $G(x) = 0$ is equivalent to $x = 0$,
(ii) $G(x) > 0$ is equivalent to $x > 0$,
(iii) $G(x) < 0$ is equivalent to $x < 0$,

then the nullclines for the classical FHN model is the same as that of the proposed model. Moreover, the existence of the pulse solution or wavetrains can be proved.

We also require the following properties for $G(x)$:

$$(i) \lim_{x \to -\infty} (G(x) - x) = 0,$$
$$(ii) \lim_{x \to \infty} G(x) \geq 0.$$

Thus, we can minimize the movement of solutions only on the right manifold as much as we want by taking b large enough. In this paper, we consider two different

cases of $G(x)$: non-monotone and monotone which satisfy the above properties in order to describe two different models:

(i) $G(x) = \dfrac{xe^{-x}}{e^{x} + e^{-x}}$, (non-monotone),

(ii) $G(x) = \dfrac{x - \sqrt{x^2 + 4}}{2} + 1$, (monotone).

The first one (i) is a non-monotone function, and the second one (ii) is a monotone function, as shown in Figs 2 and 3, respectively. We consider the value of γ neighboring its critical value γ^* where γ^* makes the v-nullcline symmetric with the u-nullcline, that is, the area bounded by the two nullclines near the upper pick and the lower pick is equal. Figure 2 shows the plots of non-monotone scaled function

$$G_b(x) = \frac{xe^{-bx}}{e^{bx} + e^{-bx}} \tag{3}$$

for four different values of b. In Fig. 3, we plot the monotone scaled function

$$G_b(x) = \frac{bx - \sqrt{b^2x^2 + 4}}{2b} + \frac{1}{b} \tag{4}$$

for four different values of b. Figure 3 shows the change of the scaled function for the change of the parameter b. We are interested to investigate the behavior of wavetrains in the above two cases. In the non-monotone case, the modified FHN model (2) becomes as follows:

$$\begin{aligned} \frac{\partial u}{\partial t} &= d_u \left(\frac{\partial^2 u}{\partial x^2} + \frac{\partial^2 u}{\partial y^2} \right) + u(1-u)(u-a) - v, \\ \frac{\partial v}{\partial t} &= d_v \left(\frac{\partial^2 v}{\partial x^2} + \frac{\partial^2 v}{\partial y^2} \right) + \varepsilon \frac{(u - \gamma v)e^{-b(u-\gamma v)}}{e^{b(u-\gamma v)} + e^{-b(u-\gamma v)}}. \end{aligned} \tag{5}$$

In the monotone case, the modified FHN model (2) becomes as follows:

$$\begin{aligned} \frac{\partial u}{\partial t} &= d_u \left(\frac{\partial^2 u}{\partial x^2} + \frac{\partial^2 u}{\partial y^2} \right) + u(1-u)(u-a) - v, \\ \frac{\partial v}{\partial t} &= d_v \left(\frac{\partial^2 v}{\partial x^2} + \frac{\partial^2 v}{\partial y^2} \right) + \varepsilon \left(\frac{b(u - \gamma v) - \sqrt{b^2(u - \gamma v)^2 + 4}}{2b} + \frac{1}{b} \right). \end{aligned} \tag{6}$$

In one-dimensional direct numerical simulation of models (5) and (6), an implicit scheme is considered. The boundary conditions are also important to get several complex phenomena in higher-dimensional problems. In our simulation, we use periodic boundary conditions on $x = 0$ and $x = L_x$, where L_x is the system size of the medium. We also use the bifurcation package WAVETRAIN (Sherratt 2012), which uses AUTO (Doedel and Kernevez 1986) to identify the location of wavetrains and the stability of

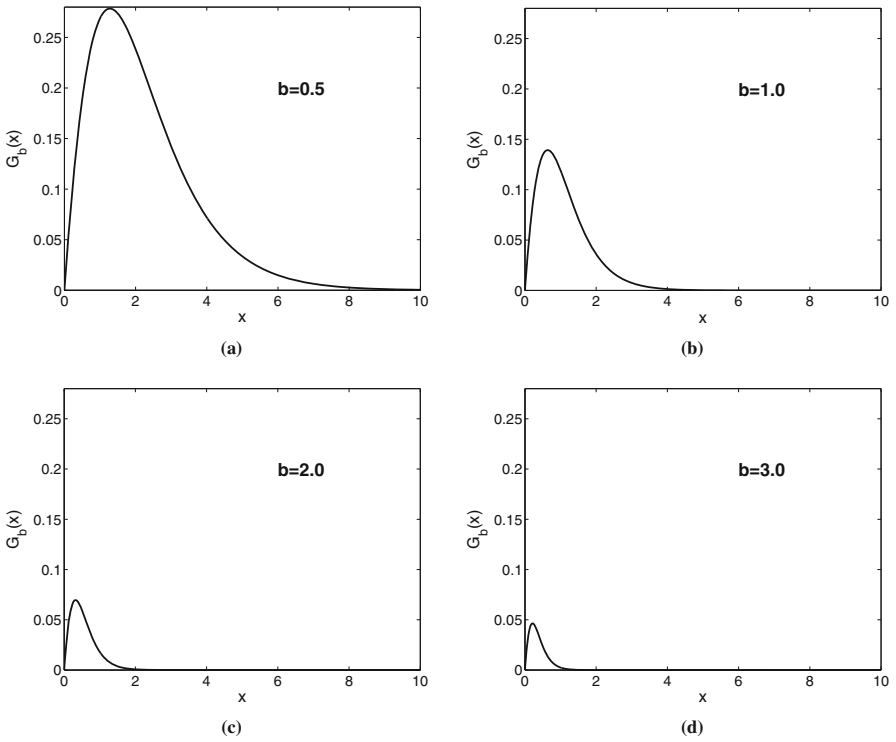

Fig. 2 Plots of non-monotone scaled function $G_b(x)$ (3) for four different values of b

Table 1 Parameters values in (5) and (6)

Parameters	a	b	γ	d_u	d_v	ε
Values	2×10^{-1}	$\cdots$	7.9	5×10^{-2}	5×10^{-3}	2.5×10^{-3}

the solutions. The parameter values of (5) and (6) are those given in Table 1, and the scaled parameter b is considered as a bifurcation parameter because it is responsible to change the reaction kinetics significantly, as shown in Figs. 2 and 3.

2.2 Method of Computation

In order to confirm the existence of wavetrains and their stability in a partial differential equation, one first needs to convert the given PDE or PDE system into an ODE system by letting $z = x - \mathbf{c}t$, where z is a traveling wave coordinate, x is space coordinate, t is the time coordinate, and $\mathbf{c}$ is the traveling wave speed. The following four-dimensional ODE system can be obtained by inserting $u(x, t) = U(z)$ and $v(x, t) = V(z)$ in either (5) or (6).

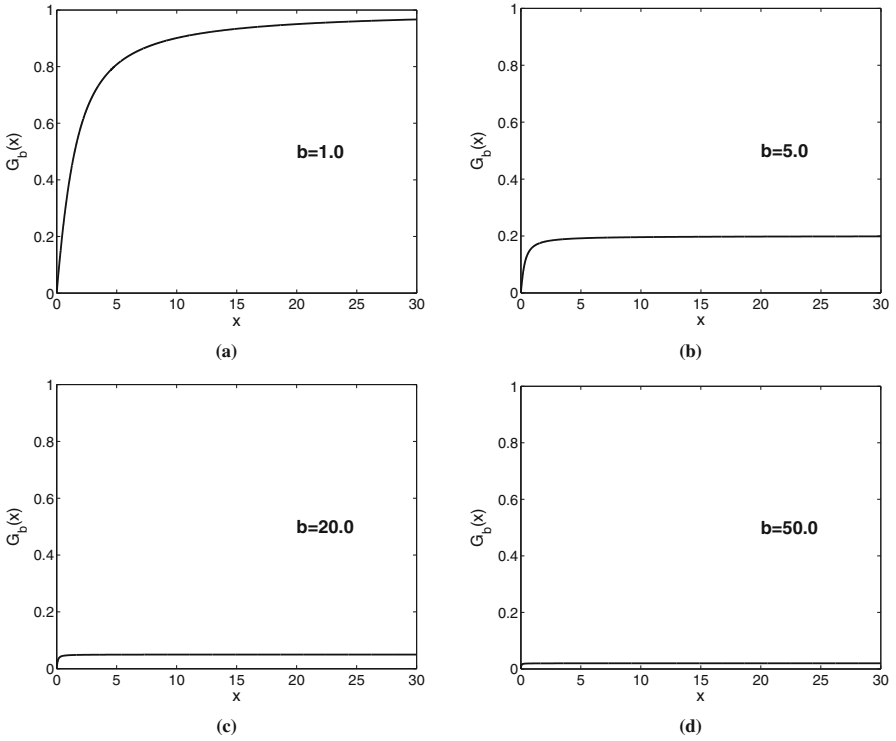

Fig. 3 Plots of monotone scaled function $G_b(x)$ (4) for four different values of b

$$\begin{aligned}
\frac{dU}{dz} &= P,\\
\frac{dP}{dz} &= (-\mathbf{c}P - U(1-U)(U-a) + V)/d_u,\\
\frac{dV}{dz} &= Q,\\
\frac{dQ}{dz} &= (-\mathbf{c}Q - \epsilon G_b(U - \gamma V))/d_v.
\end{aligned} \tag{7}$$

A wavetrain is a periodic orbit of the above system (7). To implement (5) or (6) in the bifurcation package, it is required to linearize (5) around the steady state of the system (7), $(U(z), V(z))$. Putting $u(x,t) = U(z)$ and $v(x,t) = V(z)$ in (5), while the terms having nonlinearity are neglected and it yields

$$\frac{\partial}{\partial t}\mathbf{u}_{lin} = D\frac{\partial^2}{\partial x^2}\mathbf{u}_{lin} + \mathbf{u}_{lin} \cdot \mathbf{J}_{\mathbf{F}}, \tag{8}$$

where $\mathbf{u}_{lin}(x,t) = \mathbf{u}(x,t) - \mathbf{U}(z)$. Again, substituting $\mathbf{u}_{lin}(x,t) = e^{\lambda t}\mathbf{U}(z)$ in (5) that provides the following eigenvalue problem

$$\lambda \mathbf{U} = \mathbf{c}\frac{d}{dz}\mathbf{U} + D\frac{d^2}{dz^2}\mathbf{U} + \mathbf{U}\cdot\mathbf{J_F}, \tag{9}$$

under the following boundary conditions

$$\mathbf{U}(L) = \mathbf{U}(0)\, e^{i\xi}, \text{ for some } \xi \in \mathbb{R}, \tag{10}$$

where L represents the period of the wavetrain, ξ represents the phase shift over a period of the wavetrain, $\mathbf{J_F}$ indicates the Jacobian matrix of $(f(u, v), g(u, v))$ through the wavetrain, $D = \text{diag}(d_u, d_v)$ specifies a diagonal matrix of diffusion coefficients, λ represents the eigenvalue, and $\mathbf{U}$ illustrates its corresponding eigenfunction. To investigate the bifurcations of the wavetrains, our aim is to determine the essential spectra of the wavetrains. The set consists of the eigenvalues λ so that (9) and (10) include a non-trivial solution that can be represented by the essential spectra of wavetrains. A wavetrain is treated as unstable (stable), if the imaginary axis is crossed (is not crossed) by the curvature of essential spectrum (Sherratt 2013). If the curvature crosses the imaginary axis at origin, then it is said to be an Eckhaus-type bifurcation (Sherratt 2013; Rademacher et al. 2007).

For a one-dimensional numerical approximation (i.e., in the direct PDE simulation), we seek a solution on the discrete grid points or mesh points (x_i, t_n) with $x_i = i\Delta x$, $i = 0, \cdots, N$ and $t_n = n\Delta t$, $n = 0, 1, 2, 3, \cdots$, where Δx is the mesh width and Δt is the time step. The space step in the x-direction is, therefore, defined by:

$$\Delta x = \frac{L_x}{N}, \quad N \in \mathbb{Z}, \tag{11}$$

where the size of the domain is: $0 < x < L_x$. A simple finite difference method, consisting a forward difference in time and a second order centered difference in space at the mesh point (x_i, t_n). To determine the numerical approximation of the variable in (5), we identify the grid approximation by $U_i^n \approx u(x_i, t_n)$ and $V_i^n \approx v(x_i, t_n)$ such that the full discrete approximation of U_i^n is given by:

$$\frac{U_i^{n+1} - U_i^n}{\Delta t} = d_u \frac{U_{i-1}^n - 2U_i^n + U_{i+1}^n}{\Delta x^2} + f(U_i^n, V_i^n).$$

This implies

$$U_i^{n+1} = U_i^n + \lambda_u(U_{i-1}^n - 2U_i^n + U_{i+1}^n) + f(U_i^n, V_i^n), \tag{12}$$

where

$$\lambda_u := \frac{d_u \Delta t}{\Delta x^2}. \tag{13}$$

The initial conditions are given by

$$U_i^0 = u^0(x_i), \quad 0 \le i \le N. \tag{14}$$

We use periodic boundary conditions at $i = 0$ and $i = N$. The boundary conditions for $i = 0$ and N were implemented by eliminating the ghost nodes. The ghost nodes were appearing outside the grid points, i.e., after the right end grid point for $i = 0$ and before the left end grid point for $i = N$. We eliminate the ghost nodes by using $u_{-1} = u_N$ and $u_0 = u_{N+1}$. This is that each individual value at the time step level t_{n+1} can be approximated using the previous value at time step t_n independently. This yields an explicit difference scheme. An equivalent discrete formula can also be written for V_i^n following the Eq. (12). For more details, we refer the reader to (Morton and Mayers 2005).

The stability limit $\lambda_u \leq \frac{1}{2}$ is a severe restriction in the explicit scheme, which requires a large number of time steps with limited size. However, the use of a backward difference in time gives a finite difference method that avoids such a restriction. Now, replacing the forward time difference by the backward time difference, we have:

$$\frac{U_i^{n+1} - U_i^n}{\Delta t} = d_u \frac{U_{i-1}^{n+1} - 2U_i^{n+1} + U_{i+1}^{n+1}}{\Delta x^2} + f(U_i^n, V_i^n). \tag{15}$$

This scheme is a semi-implicit scheme i.e., implicit for the diffusion and explicit for the reaction term. The scheme (15) has three values of U to be determined at the new time level $n + 1$. So, it is not possible to calculate immediately the value of U_i^{n+1}, since there is two neighboring unknown values U_{i+1}^{n+1} and U_{i-1}^{n+1}. We need to write the Eq. (15) in the following form:

$$-\lambda_u U_{i-1}^{n+1} + (1 + 2\lambda_u)U_i^{n+1} - \lambda_u U_{i+1}^{n+1} = U_i^n + f(U_i^n, V_i^n). \tag{16}$$

Now, for $i = 0, 1, 2, \cdots, N$, we have a system of $N + 1$ equations, where the number of unknowns is $N + 1$, U_i^{n+1}, $i = 0, 1, 2, \cdots, N$. The initial condition (14) that we need to consider during the simulation. The periodic boundary conditions for $i = 0$ and N are implemented by eliminating the ghost nodes, as mentioned earlier. The tridiagonal linear system of equations is solved by using an LU decomposition matrix algorithm.

3 Numerical Results and Discussion

3.1 Existence and Stability of Wavetrains for Non-monotone Scaled Function

Here, we focus on the existence of wavetrains and their stability of (5) and (6) through the continuation technique by the help of WAVETRAIN (Sherratt 2012). We find that the wavetrains in (5) bifurcate at a point, which is Eckhaus type. The solution in the fast family of the waves becomes unstable in the proposed model and subsequently bifurcates to an wave having oscillation in the simulation. These phenomena are discussed by essential spectrum, which is determined numerically. We also study the wave stability of the proposed model in the corresponding full PDE simulation.

The starting solution orbit for the continuation is calculated from the direct partial differential equation simulation. The green line in Fig. 4 indicates the locus of the

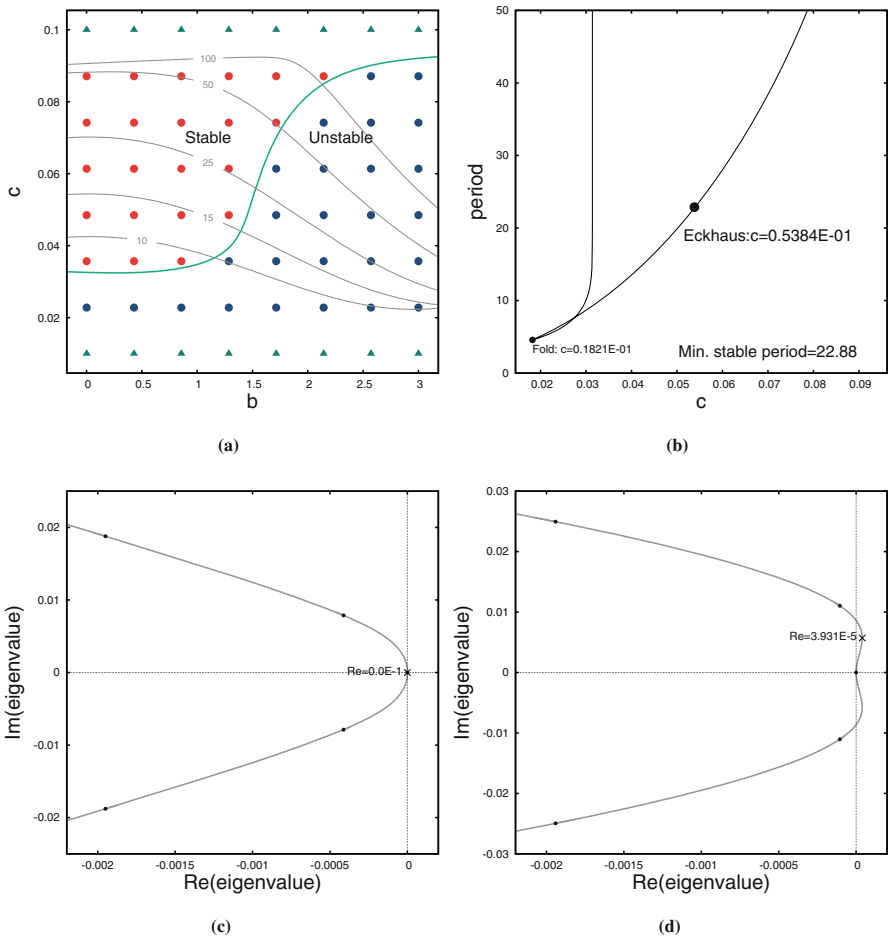

Fig. 4 **a** Existence of wavetrains and their stability of (5) in terms of b and **c**. **b** A dispersion curve of the wavetrains, when $b = 1.5$. (**c**-**d**) The essential spectra of the wavetrains before and after the Eckhaus point of (5)

Eckhaus-type bifurcation, which divides the wave existence region into two parts. One part is for stable PTWs and another part is for unstable wavetrains. Gray lines indicate the loci of the PTW solutions having periods = 100, 50, 25, 15, and 10. For constant b, the periods of wavetrains increase as the wave speed **c** increases. And again for constant wave speed **c**, periods of wavetrains increase as b increases. Our results indicate that the wave existence region whose upper boundary is the locus of the wavetrains with period infinity (homoclinic orbits) and below by the locus of the wavetrains with small periods. Figure 4b shows a bifurcation diagram of the wavetrains for $b = 1.5$, which represents the wave period, L in terms of **c**. The relation between wave period and wave speed is also termed as the dispersion curve of the wavetrains. The fold point separates the two wave branches at $\mathbf{c} = 0.01821$: one is fast and another is slow. We also find that there is an Eckhaus bifurcation point at (0.05384, 22.88).

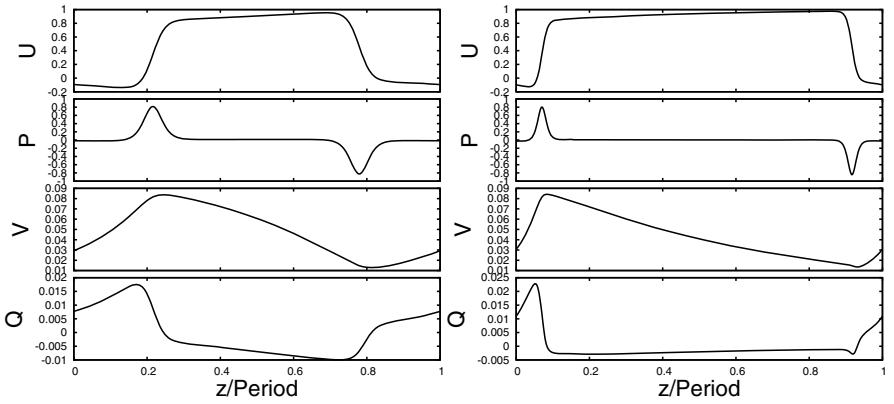

Fig. 5 Two wavetrains of (5) in Fig. 4 in terms of b and c. **a** For $b = 0.5$ and $c = 0.06$, the period is 18.78. **b** For $b = 2.0$ and $c = 0.06$ and the period is 40.99

This is the initialization of the unstable wavetrains for $b = 1.5$. Thus, the wavetrains become unstable when it is adjacent to the fold point (Bär and Brusch 2004). The wave branches in Fig. 4b start and terminate at homoclinic orbits. For the same b and $\mathbf{c}$, there are two wavetrains between the nearby homoclinic solution locus and fold point. There are also two different waves for the same period (sufficiently large), one is located on the fast branch and another one is located on the slow branch. A stable wavetrain with speed $\mathbf{c} = 0.06$, occurs at the right branch in the diagram of Fig. 4c. The imaginary line is not crossed by the spectrum, which means the wavetrain is stable. Again, an unstable wavetrain with speed $\mathbf{c} = 0.045$, occurs between Eckhaus and fold points of the diagram in the right branch (see Fig. 4d). The imaginary line is crossed by the spectrum, which indicates the wavetrain is unstable. The slow family is always unstable (Maginu 1980). Thus, our results show that in the fast family of the wavetrains with sufficiently large periods cross the stability boundary and become unstable, while these are always stable in the case of the classical FHN model.

Figure 5 displays two wavetrains of (5) in terms of b and $\mathbf{c}$ in Fig. 4. They indicate that, the periods of the wavetrains with the equal speed increases as b increases. We keep the parameter values same as chosen in Fig. 4.

In Fig. 6, we make a comparative study between the results obtained in the previous section and direct PDE simulations to observe the stability change in the wavetrains by using the non-monotone scaled function (3). In Fig. 4b, we see that the fast family of the wavetrains destabilize due to an Eckhaus-type bifurcation at $\mathbf{c} = 0.05384$ and $b = 1.5$. It is also observed that the period of the wavetrain at the bifurcation point is about $L = 22.88$. Now, we compare the stability results of the wavetrains with the corresponding direct PDE simulation. We use an implicit scheme (15), presented in Sect. 2, under periodic boundary conditions for the PDE simulation. We first consider a wavetrain having eight pulses with system size $L_x = 200$ as an initial data. As the system size is continuously decreased, we find a regular wavetrain till the Eckhaus point, i.e., in the spatial period, $l = 22.88$ (see Fig. 4b). The spatial period, l, we define

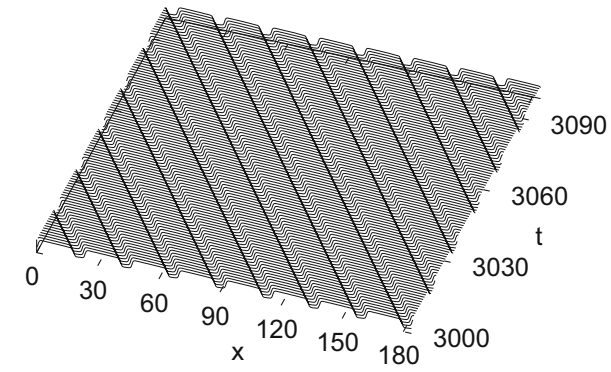

(a)

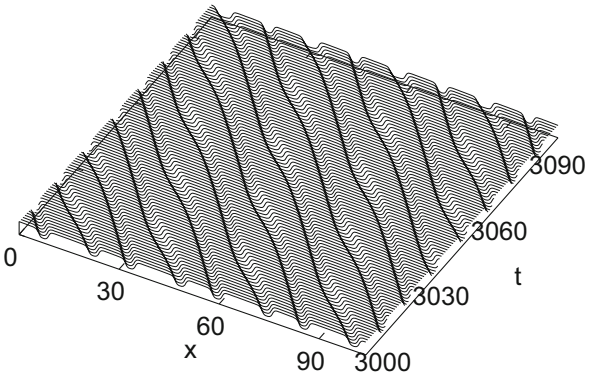

(b)

Fig. 6 Spatiotemporal patterns of (5) in one dimension, when $b = 1.5$. Transient dynamics of **a** a stable wavetrain for the spatial period $l_1 = 23$ and **b** an oscillating wavetrain due to Eckhaus bifurcation for the period $l_2 = 13$

by relationship $L_x := n \times l$, where L_x is the system size of the medium, l denotes the spatial period, and n indicates the number pulses in the wavetrain. Figure 6a shows a stable wavetrain for $L_x = 184$, i.e., $l_1 = 23$, when $l_1 > l$. This spatial period is relatively larger than that found at the bifurcation point in Fig. 4b. After that, numerical simulation reveals an oscillating wave pattern as presented in Fig. 6b for $L_x = 104$, i.e., $l_2 = 13$, when $l_2 < l$. However, the initialization of instability in the simulation is at about spatial period 20. Thus, the Eckhaus bifurcation results of the system (7) are reasonably consistent with those of the corresponding PDE simulations.

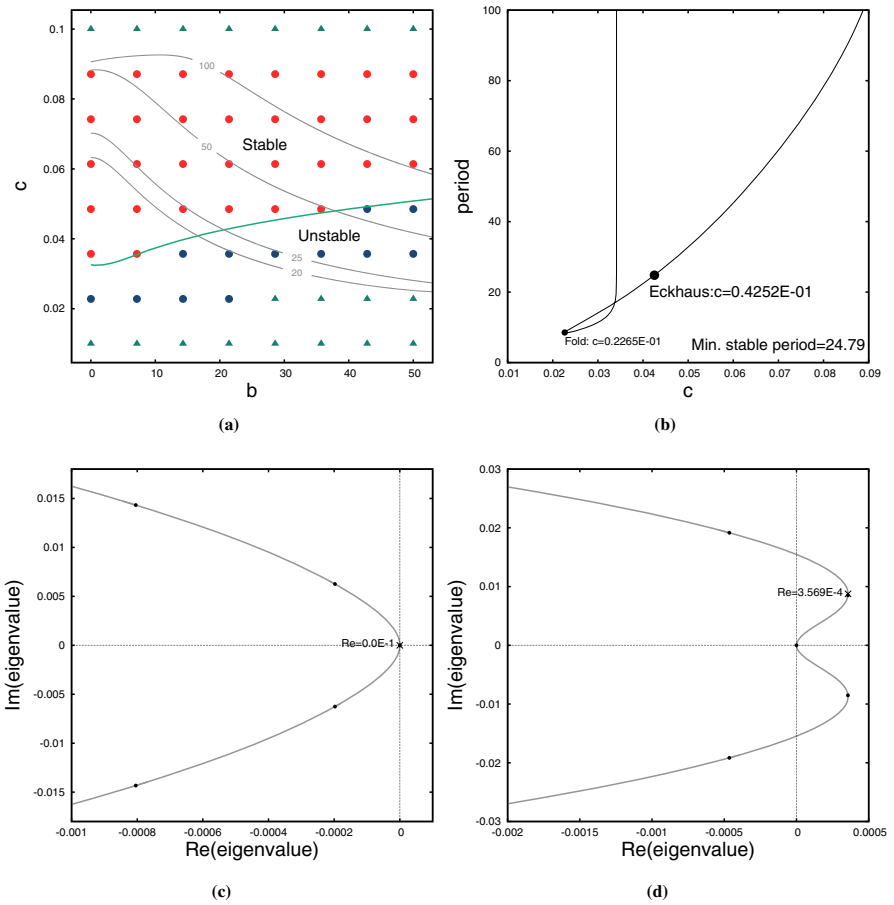

Fig. 7 **a** Existence of wavetrains and their stability of (6) in terms of b and **c**. **b** A dispersion curve of the wavetrains, when $b = 20.5$. **c-d** The essential spectra of the wavetrains before and after the Eckhaus point of (6)

3.2 Occurrence of Wavetrains and Their Stability for Monotone Scaled Function

Figure 7a shows the wave existence and stability in (6) in terms of b and **c** for the monotone scaled function, $G_b(x) = \frac{bx-\sqrt{b^2x^2+4}}{2b} + \frac{1}{b}$, mentioned above in Sect. 2. All notations and colors have the same meaning in Fig. 4. The stable and unstable waves are separated by a green line, which is the stability boundary. The loci of the wavetrains having periods = 100, 50, 25, and 20 are represented by the gray lines. Figure 7b shows a bifurcation diagram of the wavetrains for $b = 20.5$, which represents the relation between the period and the wave speed. The fold point at $\mathbf{c} = 0.02265$ separates the fast and slow branches. We also find that there is an Eckhaus bifurcation point at (0.04252, 24.79). This is the onset of the instability of the wavetrains. The wavetrains become unstable when they are near to the fold point (Bär and Brusch 2004). There are two unstable wavetrains between the fold point and the homoclinic orbit.

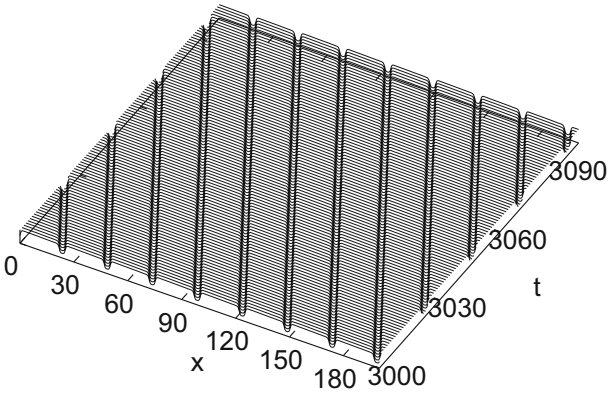

(a)

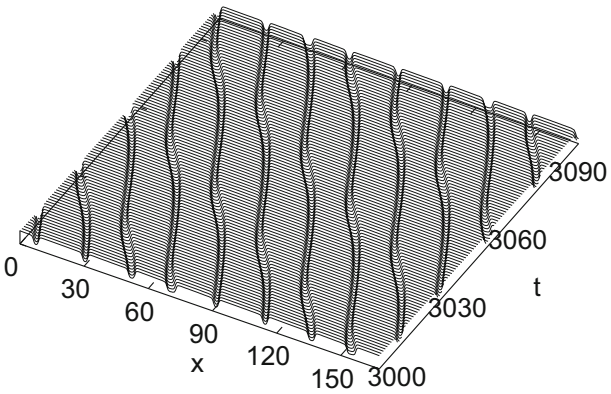

(b)

Fig. 8 Spatiotemporal patterns of (6) in one dimension, when $b = 20.5$. Transient dynamics of **a** a stable wavetrain for the spatial period $l_1 = 25$ and **b** an oscillating wavetrain due to Eckhaus bifurcation for the period $l_2 = 21$

Figure 7c represents an essential spectrum of a stable wavetrain on the dispersion curve Fig. 7b at $\mathbf{c} = 0.05$, which is a wavetrain at the fast family before the bifurcation point. The curvature of the spectrum stays at the left side, i.e., they do not cross the imaginary line that indicates the wavetrain is stable. An essential spectrum of an unstable wavetrain for $\mathbf{c} = 0.035$ is depicted in Fig. 7d, which is a wavetrain at the fast family between the fold and Eckhaus bifurcation. The curvature of the spectrum changes sign at the origin, indicating that the wavetrain is unstable of Eckhaus type (Sherratt 2013). The slow family is always unstable (Maginu 1980). Thus, our results show that the fast family of the wavetrains with small and large periods cross the stability boundary and subsequently become unstable.

In Fig. 8, we compare the direct PDE simulations and the previous results to investigate the bifurcation structure in the wavetrains by using the monotone scaled function (4). In Fig. 7b, we show that the fast family of the wavetrains destabilize due to an Eckhaus-type bifurcation at $\mathbf{c} = 0.04252$ and $b = 20.5$. It is inspected that at the bifurcation point, the period of the wavetrain is about $L = 24.79$. We now make a comparison between the stability results of the wavetrains and the corresponding direct PDE simulation. We implement an implicit finite difference scheme (15), mentioned in Sect. 2, specifying periodic boundary conditions to perform PDE simulation. For fixing initial data, we first consider a wavetrain having eight pulses with system size $L_x = 200$. We expose a regular wavetrain till the Eckhaus point, i.e., in the spatial period, $l = 24.79$, as the system size is continuously decreased (see Fig. 7b). Figure 8a demonstrates a stable wavetrain for $L_x = 200$, i.e., $l_1 = 25$, when $l_1 > l$. This spatial period is relatively larger than that obtained at the bifurcation point in Fig. 7b. After that, numerical simulation confirms an oscillating wave pattern as presented in Fig. 8b for $L_x = 168$, i.e., $l_2 = 21$, when $l_2 < l$. However, the instability initiates in the simulation at about spatial period 22. Thus, the results of the system (7) regarding the Eckhaus bifurcation have a reasonable agreement with that of the corresponding PDE simulations in Fig. 8.

3.3 Spiral Wave Existence in the Non-monotone Scaled Function

Figure 9 shows the spiral wave existence in (5) in terms of the control parameter b for the non-monotone scaled function (3). In this computations, we have considered the well-known alternating-direction implicit (ADI) method (Morton and Mayers 2005; Gani and Ogawa 2014), with Neumann boundary conditions on $[0, L_x] \times [0, L_y]$. The parameter values are the same as in Table 1. Numerical integration was done with space step $dx = dy = 0.25$ and time step $dt = 0.05$ on the grid of 800×800 elements. Figure 9a shows the initial guess of the computation that is created from the one-dimensional direct PDE simulation of (5). The initiation of the first spiral highly depends on the initial data. In this computation, we use a two-dimensional broken wavefront that is converted from a band of one-dimensional periodic traveling wave solutions. The front is located at the middle of the medium (see Fig. 9a). The spiral formation initiates from the broken wavefront and gradually takes place throughout the medium as time evolves (see Fig. 9b). The red region in Fig. 9 indicates excited state (u), and the blue region represents resting state (v) of the tissue. In the same computational settings when we increase b, the pulse width of the spiral increases. We find that when the value of the parameter crosses the Eckhaus stability boundary, the wave structure becomes anomalous. This is compatible with the one-dimensional results in Fig. 4a.

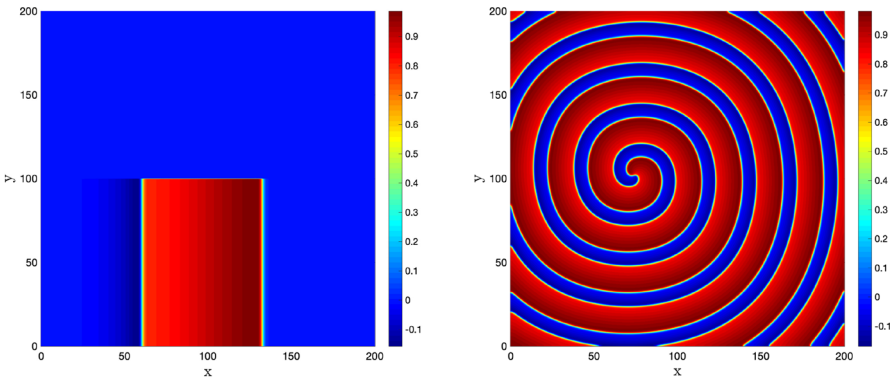

Fig. 9 Spatiotemporal spiral patterns of (5) in two dimensions for the non-monotone scaled function, when $b = 1.0$. **a** Initial data (**b**) Existence of spiral wave dynamics. Other parameters are the same as in Table 1

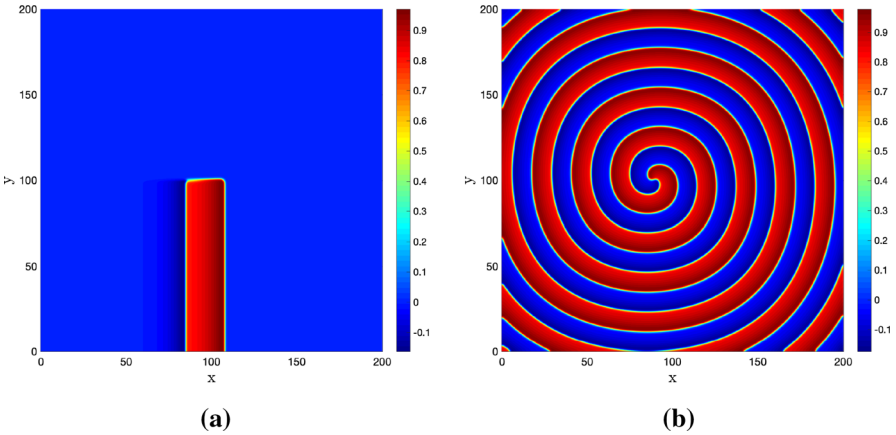

Fig. 10 Spatiotemporal spiral patterns of (6) in two dimensions for the monotone scaled function, when $b = 1.0$. **a** Initial data. **b** Existence of spiral wave dynamics. Other parameters are the same as in Table 1

3.4 Existence of Spiral Wave in the Monotone Scaled Function

Figure 10 shows the existence of spiral wave phenomenon in (6) in terms of the control parameter $b = 1.0$ for the monotone scaled function (4). Figure 10a shows the initial data of the numerical calculations that is created from the one-dimensional PDE simulation of model equations (6). Numerical integration were done with the same settings as we mentioned in the previous subsection. The first spiral initiates from the two-dimensional broken wave front, where the front is located at the middle of the medium. As time goes on, the initial spiral cover the full medium, which represents the existence of stable or regular spiral formation in the model (6). The result is consistent with the one-dimensional result in Fig. 7a.

4 Concluding Remarks

We have studied a scaled FHN-type reaction-diffusion system to understand the stability of wavetrains having sufficiently large periods and the existence of spiral wave phenomena in two different v-kinetics. We have modified the standard FHN model (1) by changing its recovery kinetics. The scaled function $G_b(x)$ is obtained from a given function $G(x)$. This paper has considered two types of $G(x)$, one is for non-monotone, and the other is for the monotone case. The modified versions of the model (1) are now taking the form as in the equations (5) and (6). It was demonstrated in Figs. 4 and 7 that one scaled parameter b of (5) and (6) causes instabilities of the wavetrains. Our results indicated that the periods of the wavetrains increase as its speed $\mathbf{c}$ increases when the scaled parameter b is constant. At a constant speed, $\mathbf{c}$ of the wavetrain, the periods of the wavetrains increase as the control parameter b increases (see Figs. 4 and 7). It is known that for the classical FHN model, the wavetrains having adequately large periods are always stable (Maginu 1980; Gani and Ogawa 2015). However, in the proposed models, (5) and (6), it is observed that in the two-dimensional bc-parameter plane, the periodic traveling waves having sufficiently large periods cross the boundary of Eckhaus bifurcation (see Figs. 4a and 7a). These results are a new contribution to study of the FHN model of nerve cell dynamics. In the direct PDE simulation, we observed that a stable wavetrain bifurcates to an oscillating wavetrain when the wave crosses the boundary of Eckhaus-type bifurcation (see Figs. 6 and 8). Oscillating wavetrain is an interesting pattern of solution as it is observed in the irregular nerve cell and irregular heart cell dynamics (Gani and Ogawa 2016). Furthermore, numerical results have revealed the existence of spiral waves (see Figs. 9 and 10) for both non-monotone and monotone cases of $G(x)$. Numerous experimental and computational studies exhibit that a spatial scheme can be produced by the spiral waves that leads to the construction of cortical oscillations in the nerve cells of many systems from invertebrates to mammals (Huang 2004; Davidenko et al. 1992; Ermentrout and Kleinfeld 2001a; Gani and Ogawa 2014; Yu et al. 2010; Ma et al. 2009). Spirals have a significant role to synchronize oscillatory dynamics over nerve cells. Numerical results discussed in Sect. 3 possess a reasonable agreement with the spatiotemporal dynamics of a neuron as numerous studies exhibit clinical investigations of spatiotemporal characteristics of nerve cell in different species (Gray 1989; Lechleiter 1991; Wu et al. 2001; Jalife 2003). Finally, it is commendable that this modified FHN model presented here can enrich the present research scale of the model-aided understanding of nerve cell dynamics.

Acknowledgements It is acknowledged the support provided by the GCOE program entitled "Formation and Development of Mathematical Sciences Based on Modeling and Analysis", of the Meiji University, Japan, where this work was carried out.

References

Bär M, Brusch L (2004) Breakup of spiral waves caused by radial dynamics: eckhaus and finite wavenumber instabilities. New J Phys 6:5

Bauer S, Röder G, Bär M: Alternans and the influence of ionic channel modifications: cardiac three–dimensional simulations and one-dimensional numerical bifurcation analysis. Chaos: An Interdiscip J Nonlinear Sci **17**, 015104 (2007)

Bierman SM, Fairbairn JP, Petty SJ, Elston DA, Tidhar D, Lambin X (2006) Changes over time in the spatiotemporal dynamics of cyclic populations of field voles (microtus agrestis l.). Am Nat 167(4):583–590

Bordiougov G, Engel H (2006) From trigger to phase waves and back again. Phys D 215:25–37

Bordyugov G, Engel H (2006) Creating bound states in excitable media by means of nonlocal coupling. Phys Rev E 74:016205

Bordyugov G, Fischer N, Engel H, Manz N, Steinbock O (2010) Anomalous dispersion in the belousov-zhabotinsky reaction: experiments and modeling. Phys D: Nonlinear Phenom 239(11):766–775

Davidenko JM, Pertsov AV, Salomonsz R, Baxter W, Jalife J (1992) Stationary and drifting spiral waves of excitation in isolated cardiac muscle. Nature 355(6358):349–351

DeVille REL, Eijnden EV (2007) Wavetrain response of an excitable medium to local stochastic forcing. Nonlinearity 20(1):51

Doedel EJ, Kernevez J (1986) Auto: software for continuation and bifurcation problems in ordinary differential equations. Applied Mathematics Report, California Institute of Technology, Pasadena, USA

Echebarria B, Röder G, Engel H, Davidsen J, Bär M (2011) Supernormal conduction in cardiac tissue promotes concordant alternans and action potential bunching. Phys Rev E 83:040902

Epstein IR, Showalter K (1996) Nonlinear chemical dynamics: oscillations, patterns, and chaos. J Phys Chem 100(31):13132–13147

Ermentrout GB, Kleinfeld D (2001) Traveling electrical waves in cortex: insights from phase dynamics and speculation on a computational role. Neuron 29(1):33–44

Ermentrout GB, Kleinfeld D (2001) Traveling electrical waves in cortex: insights from phase dynamics and speculation on a computational role. Neuron 29(1):33–44

FitzHugh R (1961) Impulse and physiological states in theoretical models of nerve membrane. Biophys. J. 1:445–465

Gani MO, Ogawa T: (2014). Alternans and spiral breakup in an excitable reaction-diffusion system: a simulation study. Int Sch Res Not **2014**(459675)

Gani MO, Ogawa T (2015) Instability of periodic traveling wave solutions in a modified FitzHugh-Nagumo model for excitable media. Appl Math Comput 256:968–984

Gani MO, Ogawa T (2016) Stability of periodic traveling waves in the aliev-panfilov reaction-diffusion system. Commun in Nonlinear Sci Numer Simul 33:30–42

Gorelova NA, Bureš J (1983) Spiral waves of spreading depression in the isolated chicken retina. J neurobiol 14(5):353–363

Gray CM (1989) Singer W?: Stimulus-specific neuronal oscillations in orientation columns of cat visual cortex. Proceed National Acad Sci 86(5):1698–1702

Hecke MV (2003) Coherent and incoherent structures in systems described by the 1d cgle: experiments and identification. Phys D: Nonlinear Phenom 174(1):134–151

Huang X et al (2004) Spiral waves in disinhibited mammalian neocortex. J Neurosci 24(44):9897–9902

Izhikevich EM : (2007). Dynamical systems in neuroscience. MIT press

Jalife J (2003) Rotors and spiral waves in atrial fibrillation. J Cardiovasc Electrophysiol 14(7):776–780

Kopell N, Howard LN (1973) Plane-wave solutions to reaction-diffusion equations. Stud Appl Math 52:291–328

Lechleiter J et al (1991) Spiral calcium wave propagation and annihilation in xenopus laevis oocytes. Science 252(5002):123–126

Ma J, Jia Y, Yi M, Tang J, Xia YF (2009) Suppression of spiral wave and turbulence by using amplitude restriction of variable in a local square area. Chaos, Solitons & Fractals 41(3):1331–1339

Maginu K (1980) Existence and stability of periodic travelling wave solutions to nagumo's nerve equation. J Math Biol 10(2):133–153

Meron E (1992) Pattern formation in excitable media. Phys Rep (Rev sect Phys Lett) 218:1–66

Morton KW, Mayers DF : (2005). Numerical solution of partial differential equations: an introduction. Cambridge university press

Nagumo JS, Arimoto S, Yoshizawa S (1962) An active pulse transmission line simulating nerve axon. Proc IRE 50:2061–2071

Oreanu CR, Georgescu A, Eanu NG : (2000) The FitzHugh-Nagumo Model: Bifurcation and Dynamics. Kluwer Academic Publishers

Rademacher JD, Sandstede B, Scheel A (2007) Computing absolute and essential spectra using continuation. Phys D: Nonlinear Phenom 229(2):166–183
Ranta E, Kaitala V (1997) Travelling waves in vole population dynamics. Geochim Cosmochim Acta 61:3503–3512
Saarloos WV (2003) Front propagation into unstable states. Phys report 386(2):29–222
Sakaguchi H, Maruyama T (2008) Elimination of pulses and spirals by external forces in luo-rudy model. J Phy Soc Japan 77:1–5
Sherratt JA (2012) Numerical continuation methods for studying periodic travelling wave (wavetrain) solutions of partial differential equations. Appl Math & Comput 218:4684–4694
Sherratt JA (2013) Numerical continuation of boundaries in parameter space between stable and unstable periodic travelling wave (wavetrain) solutions of partial differential equations. Adv Comput Math 39:175–192
Sherratt JA, Lord GJ (2007) Nonlinear dynamics and pattern bifurcations in a model for vegetation stripes in semi-arid environments. Theor popul biol 71(1):1–11
Sherratt JA, Smith MJ (2008) Periodic travelling waves in cyclic populations: field studies and reaction-diffusion models. J Royal Soc Interface 5(22):483–505
Steinberg V, Fineberg J, Moses E, Rehberg I (1989) Pattern selection and transition to turbulence in propagating waves. Phys D: Nonlinear Phenom 37:359–383
Vanag VK, Epstein IR (2008) Design and control of patterns in reaction-diffusion systems. Chaos?:An Interdiscip J Nonlinear Sci 18(2):026107
Verkhratsky A, Orkand RK, Kettenmann H (1998) Glial calcium: homeostasis and signaling function. Physiol Rev 78(1):99–141
Wu JY, Guan L, Bai L, Yang Q (2001) Spatiotemporal properties of an evoked population activity in rat sensory cortical slices. J Neurophysiol 86(5):2461–2474
Yu G, Ma J, Jia Y, Tang J (2010) Dynamics of spiral wave in the coupled hodgkin-huxley neurons. Int J Modern Phys B 24(23):4555–4562